Coral Reefs (2025) 44:273–289
https://doi.org/10.1007/s00338-024-02603-8

Emergent coral reef patterning via spatial self-organization

Haiwei Xi[1] · Xiaoli Dong[2] · Ved Chirayath[1] · Arthur C. R. Gleason[1] · Sam J. Purkis[1]

Received: 2 August 2024 / Accepted: 21 November 2024 / Published online: 7 December 2024

Abstract Regularly patterned reef ridges develop in the lagoons of at least one-third of Earth's coral reefs. The interactions between corals and their environment, occurring at scales from millimeters to meters, can lead to self-organized spatial patterns spanning hundreds of meters to kilometers. To understand the mechanism behind pattern formation, we first characterize these spatial patterns using satellite imagery from 63 sites across the Atlantic, Pacific, and Indian Oceans. Next, we develop a generalized Turing morphogenesis model. Corroborated by observed spatial patterns, results from our numerical model suggest that patterned ridges develop through a four-phase trajectory, dictated by changes in the lagoon's hydrodynamic regime. Initially, after an atoll lagoon forms, the first colonizing reefs establish as isolated pinnacles. These pinnacles then evolve into low-relief ridges and eventually form semi-enclosed inter-ridge ponds. In the terminal phase, a dense interconnected, branching, and rejoining ("anastomosing") pattern of reef ridges develop into a network, fully enclosing the ponds. Once enclosed, wind- and tide-induced currents are significantly reduced. Since corals rely on flow for feeding and shedding metabolites, ridge development stalls, and the pattern stabilizes. By combining empirical observations from around the world with a theoretical model, our study reveals the mechanism of reef pattern formation. Such a mechanistic understanding enables the use of emergent reef patterns to identify reef stress at the coral colony scale.

✉ Sam J. Purkis
spurkis@earth.miami.edu

[1] Rosenstiel School of Marine, Atmospheric, and Earth Science, University of Miami, Coral Gables, USA

[2] Department of Environmental Science and Policy, University of California Davis, Davis, USA

Keywords Coral Reef Morphogenesis · Spatial Self-Organization · Turing Model · Hydrodynamic Feedbacks · Remote Sensing

Introduction

Over the last 4 decades, half of Earth's reefs have died (Eddy et al. 2021). The so-called "reef crisis" is a symptom of a planet slowly, inexorably overheating (Woodhead et al. 2019). Reefs are facing transitions that are likely catastrophically abrupt and irreversible (Stuart-Smith et al. 2018; Williams and Graham 2019). Reefs evidently have critical thresholds—so-called tipping points—beyond which the ecosystem shifts abruptly from a biodiverse state, to one that is moribund and low in species richness (Purkis and Riegl 2005; Riegl et al. 2012, 2015). Such shifts have societal consequences. More than one billion people rely on coral reefs for protein, reefs protect coastlines from storms and tsunamis, and they yield bioactive molecules for new medicines (Hughes et al. 2018). It is challenging to predict critical transitions because the system may show little change before the tipping point is reached. Detecting the subtle signals of an impending transition is especially hard for reefs. Timeseries from traditional diver-monitoring rarely extend back more than 20 years (Aronson et al. 2002; Gardner et al. 2003); too short to track the natural variability of such a complex ecosystem. A shortcut to predicting tipping points in reefs would therefore be desirable in order to speed the pathway to effective conservation. Tipping points often align with the emergence of coherent patterns in ecosystem architects. If such patterns appear at spatial scales detectable by remote sensing, as we believe for coral reefs, impending tipping points could be identified from orbit.

Despite distinctive differences in scale, biology, and environment, many spatially self-organized ecosystems show striking similarities in terms of the coherent patterns they form (Purkis and Kohler 2008; Rietkerk and van de Koppel 2008; Budd et al. 2016; Purkis et al. 2016). Spatial self-organization is the process where local interactions give rise to large-scale regular spatial patterns from disordered initial conditions. Examples can be found in mussel beds (van de Koppel et al. 2005; Liu et al. 2014), semi-arid vegetation (Couteron and Lejeune 2001), wetlands (Quintero and Cohen 2019; Dong et al. 2021)—including mangroves (van Maanen et al. 2015), seagrass meadows (van Der Heide et al. 2010; van de Vijsel et al. 2023), marsh tussocks (van de Koppel and Crain 2006), microbially-precipitated carbonates (Petroff et al. 2011; Xi et al. 2022), sand flats (Coco and Murray 2007), and *Halimeda* bioherms (McNeil et al. 2021; Reolid et al. 2024). It has also been well-established that spatial self-organization by corals can deliver coherent patterning (Mistr and Bercovici 2003; Rietkerk and van de Koppel 2008; Purkis et al. 2010; Blakeway and Hamblin 2015; Purkis et al. 2015; Zlatarski and Greenstein 2020; van der Kaaden et al. 2021, 2023; Génin et al. 2024)—the focus of our study.

To investigate the specific mechanism underlying pattern formation of coral reefs, Mistr and Bercovici (2003) proposed a theoretical model. It predicted regularly-spaced reefs oriented perpendicular to water flow, as indeed has been documented at colony scale (Helmuth et al. 1997) and at reef-scale (Purkis et al. 2016). However, their model fails to reproduce reticulated reef patterning in atoll lagoons, as described by Woodroffe (2011) and Purkis et al. (2015). Reticulated reefs were initially interpreted to be a manifestation of antecedent seafloor topography (Purdy 1974; Purdy and Bertram 1993; Purkis et al. 2010). However, recent drilling and seismic surveys show that this reticulate pattern is not a living reef veneer of an underlying seafloor template, but instead capable of developing independently on a flat featureless seabed (Schlager and Purkis 2015; Purkis et al. 2016)—that is, the patterned reef ridges are modern, built via biological processes, not a mere manifestation of the underlying geological templates (Salas-Saavedra et al. 2018). In the context of Earth as a planetary analog for oceans across the solar system, such patterning may therefore be particularly useful in the detection of extant or fossilized biosignatures against abiotically generated geological formations (Chirayath et al. 2022).

Regular patterns in many ecosystems evolve on human timescales (Scheffer et al. 2001; van de Koppel et al. 2005; Quintero and Cohen 2019). Coral reefs behave differently in at least two aspects: First, their growth is exceptionally slow and reticulated coral ridges take millennia to develop (Hopley 1982; Marshall and Davies 1982; Guilcher 1988; Blakeway and Hamblin 2015). Second, reefs are built from limestone, laid down by their primary architect, corals, along with a myriad of other calcifying organisms. The patterned reefs which emerge from the interaction of these architects with each other, and their environment, are rigid and wave resistant. The pattern can evolve through time as the reefs expand vertically and horizontally, but this evolution is additive to the structure. This is in contrast to a self-organized seagrass meadow, for instance, which can evolve by patch expansion via growth, but also by patch contraction via mortality (e.g., van de Vijsel et al. 2023). Reefs do not contract, at least not on the timescales relevant to this study, though bioerosion does continuously convert small portions of the reef framework to sediment, a process which, in healthy ecosystems, is balanced by reef growth (Perry et al. 2008; Dee et al. 2024). The idea of reef permanence is central to the conceptual model of patterned reef formation proposed by Purkis et al. (2016), whereby individual patch reefs coalesce to form ever denser networks of interconnected ridges, similar to the “juvenile", “mature", and “senile" phases of reef development proposed by Hopley (1982) and captured in the typology published by Rowlands et al. (2014).

In this study, we aim to: (1) characterize the coherent spatial patterns of coral reefs and (2) investigate the mechanism which deliver that patterning. We first assembled satellite imagery for 63 coral reefs spanning the Atlantic, Pacific, and Indian Oceans which display coherent reef patterns. The spatial patterns were analyzed using directional connectivity and radial spectrum analysis. Second, we constructed a generalized Turing-type reaction–diffusion model to reproduce the observed natural reef patterns and used this model to unravel the complexity arising from spatial–temporal interactions between reef growth, sedimentation, and water flow. This study contributes to our overall goal of relating the spatial patterns of coral reefs to their state of development and health.

Methods

Reef mapping from satellite imagery

To compile a robust dataset of patterned reefs, we surveyed global reef provinces using Google Earth, identifying 63 sites that captured the full spectrum of global reef patterns (Fig. 1). All sites are in waters shallower than 10 m, enabling clear satellite imaging, and include atoll, platform, barrier, and fringing reefs. Next, PlanetScope imagery acquired between 2020 and 2023 was assembled for those 63 sites. These satellite data have a spatial resolution of 3×3 m in the visible spectrum and images were selected from cloud-free days with calm seas, such that the seabed was optimally resolved. We radiometrically and atmospherically corrected the imagery using the protocols established in Purkis et al.

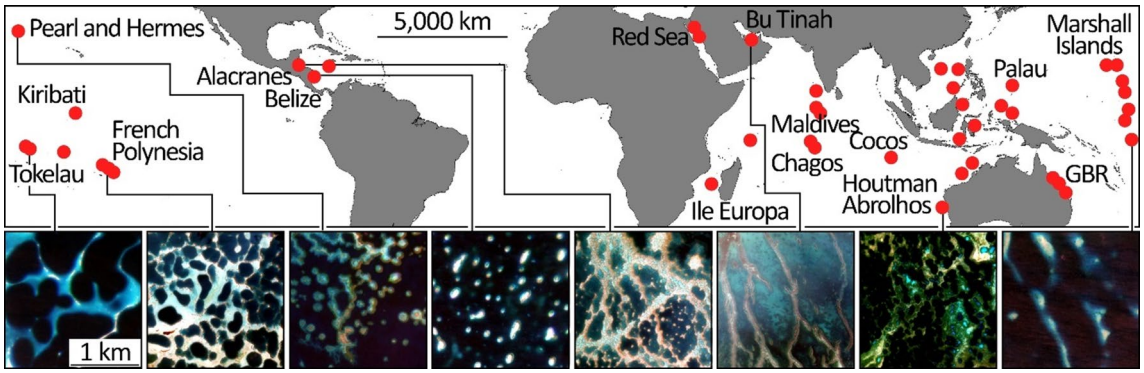

Fig. 1 Locations of the 63 coral reefs where reef patterns were satellite mapped. For each site, a representative 2×2 km area was mapped to capture reef patterning. Eight representative sites for reference

(2019). From each reef site, a 2×2 km image subset was extracted which captured the reef patterning characteristic of that site. These subsets were assembled and carried forward for pattern quantification.

Reef mapping and reef pattern extraction

To map reef morphology for each 2×2 km image, we adopted the workflow developed by Purkis et al. (2019). First, a bathymetry map was spectrally derived from the PlanetScope image subsets using the multi-linear regression method described in Kerr and Purkis (2018) (Fig. 2). Next, using the satellite imagery and this bathymetry map (Fig. 2bc), the reefs were mapped using an "object-based" classifier that utilizes the spectral and textural content of the input data (Purkis et al. 2019). These objects were subsequently classified into reef edge, reef interior, and pond, based on their different spectral/textural signatures, shape, and contextual relationships with surrounding classes (Fig. 2d).

The reef structure, including patch reefs, ridges, and pinnacles, was classified into two groups—"reef edge" and "reef interior". The edge of the reef structure is the prime locus of active coral growth, where hydrodynamic shear is high, thinning the diffusive boundary layer between reef and the surrounding water mass (Schlager and Purkis 2015). Thus, the reef edge has amplified access to nutrients and is unlikely to be buried by sediment. The reef interior, by contrast, is disadvantaged by low hydrodynamic shear and therefore often veneered with sediment, which gives it a brighter color in satellite imagery (Fig. 2ab). The lagoon floor, the background to the reef structure, was classified as being composed of "ponds", so named because of the ponded morphology created when reef ridges encircle portions of lagoon floor. We consider our "ponds" to be synonymous with the "cells" of Blakeway and Hamblin (2015). Finally,

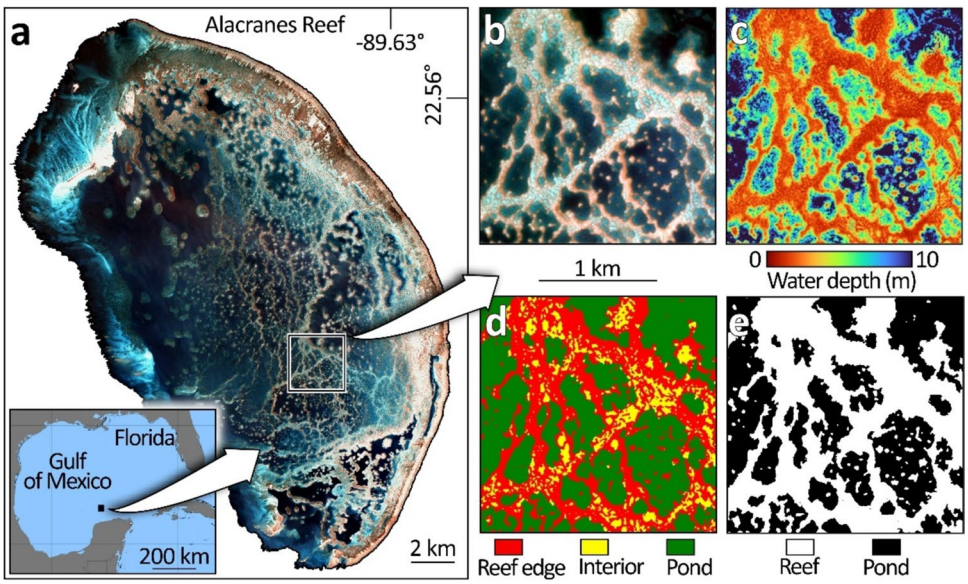

Fig. 2 Development of binary maps of reef morphology: **a** Alacranes Reef situated in the Gulf of Mexico provides a textbook example of reticular coral ridges. In this example, as in the 63 reefs mapped globally, a representative 2×2 km subset of satellite image (**b**) was selected, from which bathymetry was spectrally retrieved (**c**). On the basis of this pair of data layers, the imagery was mapped into three benthic classes (**d**), reduced to a binary morphology map (**e**) carried forward for statistical pattern analysis

as the reef edge and reef interior are both part of the reef structure, they were merged to yield a binary map consisting of "reef" and "pond" (Fig. 2d). We then analyzed the spatial patterns of these binary maps across the 63 sites.

Reef directional connectivity index and principal axis ratios

We quantified reef connectivity and orientation using the directional connectivity index (DCI) (Larsen et al. 2012). First, using the Image Processing Toolbox in MATLAB® (version 2023b), a skeleton representation of reef feature was extracted for each "reef" patch in the 63 binary maps. This extraction is accomplished by progressively removing edge pixels without allowing the patch to break apart. Based on the extracted skeleton, the DCI was computed by successively rotating the binary image with respect to the N-S grid of PlanetScope pixels. DCI was computed at each 10° increment of rotation. This index ranges from 0 to 1, with 1 denoting complete reef connectivity in a given direction. When DCI = 0, by contrast, the reefs within the binary map display zero connectivity in the specified direction.

To demonstrate how DCI performs, consider the results for Glover's Reef (Caribbean), Alacranes Reef (Gulf of Mexico), and Atafu Atoll (S. Pacific) (Fig. 3a–c). These sites display an increasing connectivity from scattered patch reefs (Glover's), to elongated reef ridges (Alacranes), and well-developed networks of ridges (Atafu). Such a transition in connectivity is captured by the direction-averaged DCI—hereafter termed "mean DCI". For example, the mean DCI values of Glover's Reef, Alacranes Reef, and Atafu Atoll are 0.06, 0.24, and 0.63, respectively. Furthermore, to characterize the isotropy and directionality of reef patterning, we followed Purkis et al. (2007) and calculated the principal axis ratio (PAR) for each DCI polar plot, which is the maximum ratio of the DCI pair that describes two orthogonal cardinal directions. An isotropic pattern (i.e., one that lacks directionality) returns similar DCI values in all directions, i.e., a PAR close to 1. Reef patterns with a preferred orientation, by contrast, show a marked increase of DCI in the dominant direction of reef orientation, leading to a PAR value much greater than 1. For instance, the PAR of the Alacranes Reef (PAR = 3.10) is much higher than that of the Atafu Atoll (1.16; Fig. 3).

Spectral analysis of reef patterns and clustering

The first metric which we used for pattern characterization was reef fraction, defined as the proportion of each 2 × 2 km binary map classified as "reef". As a second metric of

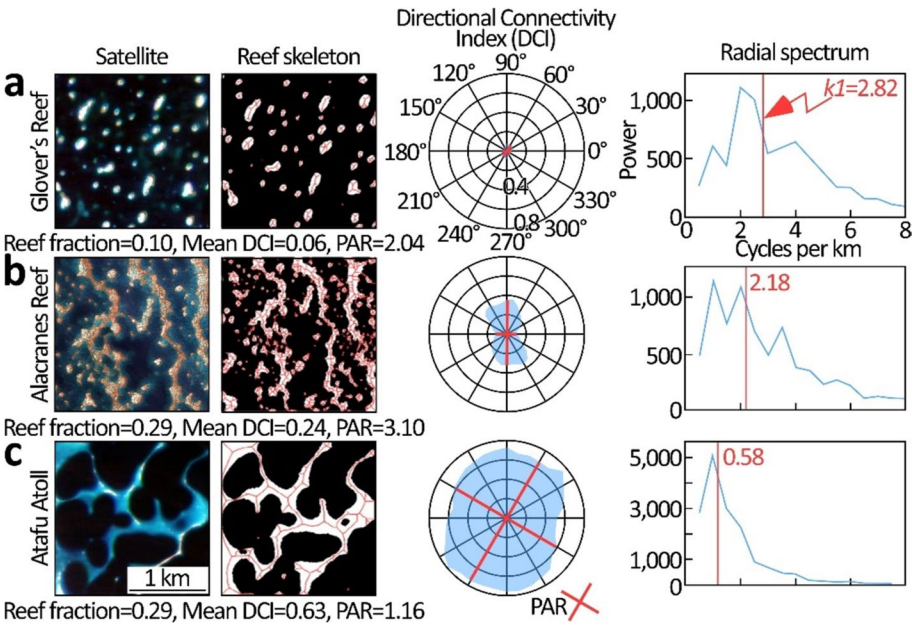

Fig. 3 Pattern analyses of reef ridge morphology from three contrasting sites—Glovers Reef (**a**), Alacranes Reef (**b**), and Atafu Atoll (**c**). Directional connectivity index (DCI) is computed from a skeletonized representation of the reef morphology. Mean DCI is the average DCI iteratively computed every 10° of rotation. Note how the isolated patch reefs at Glover's return low mean DCI (0.06), the partially connected networks of Alacranes return an intermediate value (0.24), and the completely connected networks of Atafu return the highest mean DCI (0.63). Principal axis ratio (PAR) is extracted from the DCI polar plots and characterized the degree of isotropy in the alignment of reef ridges—the Alacranes ridges have preferred orientation, those in Glover's Reef do not. Radial spectrum analysis provides the characteristic wavenumber (*k1*) of the reef patterns, taken as the weighted average of the entire spectrum signal in units of cycles per km (*red* vertical lines)

pattern characterization, we used radial spectrum analysis (Renshaw and Ford 1984) to determine the dominant scales of variability in reef morphology within the binary maps created for our 63 coral reef sites. This analysis identifies dominant spatial frequencies in pattern, as accounted for by a cosine wave repeating k times (termed the "wavenumber") along a given direction (θ). A radial power spectrum ($S(k)$), meanwhile, shows the dominant number of waves that fits a given pattern, irrespective of direction (Fig. 3). Reefs arranged in a regular spatial pattern with a characteristic wavelength will have a dominant wavenumber peak in a radial spectrum plot. By contrast, a random pattern lacks well-defined spectral peaks. To identify dominant k for our 63 reef sites, we followed Bastiaansen et al. (2018) and computed their weighted average power spectra of the first 32 wavenumbers.

As with the DCI, we can demonstrate the utility of spectral analysis for pattern quantification using the same three reef sites as before—Glover's Reef, Alacranes Reef, and Atafu Atoll (Fig. 3a–c). Here, the characteristic wavenumber ($k1$) displays a decreasing trend from scattered patch reefs (Glover's), to elongated reef ridges (Alacranes), to well-developed networks of ridges (Atafu). This trend is due to a progressive shift of spectral power from high to low wavenumber. The patch reef dominated pattern (Glover's) shows a strong peak at 2 cycles per km. In comparison, the pattern of mixed patch reefs and ridges present at Alacranes shows strong peaks at 1 and 2 cycles per km, whereas Atafu Atoll, which contains highly reticulated reef ridges (and no patch reefs) returns a single peak at 1 cycle per km. Regardless of the difference in $k1$, the spectral analysis suggests that the reef patterns at all three sites are periodic.

In order to classify the mapped reefs into groups with similar patterns, we employed K-means clustering. This method uses an iterative algorithm to split a multivariate dataset into distinct, non-overlapping subgroups (MacQueen 1967). The inputs to this clustering algorithm include the site-specific reef fraction, mean DCI, and characteristic wavenumber ($k1$).

Generalized reaction–diffusion model for reef morphogenesis

Reef growth model

To investigate the mechanism giving rise to the reef patterns mapped from satellite, we developed a generalized reaction–diffusion model capturing the processes and hydrodynamic feedbacks hypothesized to effect reef growth. In the model, reef growth (B) and the sediment shed by the reef (S) affect bathymetry (z), which modulates hydrodynamic flow. Altered flow, in turn, affects rates of reef growth and sedimentation, thereby setting up a series of feedbacks between reef growth, sediment production, and flow dynamics.

Changes in living reef biomass density (B, ton/m^2) integrate the growth of individual coral colonies, their mortality, and lateral reef expansion:

$$\frac{\partial B}{\partial t} = r f_B(u_*)\left(\frac{W_z - z}{W_z - z + k_s}\right)B - Bm + D_1 * \left(\frac{\partial^2 B}{\partial x^2} + \frac{\partial^2 B}{\partial y^2}\right) \quad (1)$$

where r is the intrinsic reef growth rate (ton year^{-1} m^{-2}), f_B is a function describing the effect of the hydrodynamic shear velocity (u_*, m/s), serving as a proxy for the turbulence of flow (Duncan et al. 1960), on reef growth rate, z is the elevation of the coral surface (m), $(W_z - z)$ describes the distance between the sea surface and the seabed (i.e., water depth; here W_z is a constant describing the depth of water in the system without coral reef or sediment accumulation; it is set at 10 m at model initiation), k_s (m) is the water depth at which reef growth is at the half maximum rate, so set because vertical reef growth rate (i.e., increases in z) diminishes as the reef aggrades to sea level (Bosence and Waltham 1990), m is the specific mortality loss of reef biomass density (year^{-1}), and D_1 is the diffusion coefficient describing the lateral spreading of reef biomass (m^2 year^{-1}) (Holmes et al. 1994).

It has been well-established that reef growth is enhanced by high flow rates, which increase nutrient access and sweep away nuisance sediment (Atkinson et al. 2001; Hearn et al. 2001; Schutter et al. 2010; Schlager and Purkis 2013). Since our mapped sites are all situated in quiescent lagoonal environments, we assumed a linear relationship between the shear velocity (u_*, m/s) and rate of reef growth (Eq. 2), such that growth rate increases proportionally with shear velocity, until reaching a critical shear velocity (u_c, m/s), beyond which shear velocity is no longer a limiting factor for reef growth:

$$f_B(u_*) = \begin{cases} \frac{u_*}{u_c} & u_* \le u_c \\ 1 & u_* > u_c \end{cases} \quad (2)$$

Dead reefs gradually decompose to sediments due to bioerosion, which we assume to proceed at a relatively slow, constant rate (Masiero et al. 2020). Sediment shed from the reef structure is transported down slope by gravity, following the bathymetric surface and redeposited in the bathymetric lows adjacent to the source reef, a process approximated by diffusion. Thus, sediment thickness (S, m) evolves as follows:

$$\frac{\partial S}{\partial t} = cBm + D_2 * \left(\frac{\partial^2 z}{\partial x^2} + \frac{\partial^2 z}{\partial y^2}\right) \quad (3)$$

where c is a conversion constant of dead reef to sediments (m^3/ton) and D_2 is the sediment diffusion coefficient.

Changes in seabed elevation (z, m) are affected by changes in reef biomass and sedimentation:

$$\frac{\partial z}{\partial t} = \frac{1}{\gamma}\frac{\partial B}{\partial t} + \frac{\partial S}{\partial t} \tag{4}$$

where γ is the bulk density of reef framework (ton m^{-3}).

Hydrodynamic flow

To simulate a flow velocity field, we applied a two-dimensional depth-averaged hydrodynamic module. Initially developed by Baker (2003) and later applied in Waltham (2008), this module assumes conservation of water volume, a logarithmic relationship between flow velocity and water depth, and steady-state flows that follow the minimum shear stress. We contend the steady flow assumption to be reasonable as the water residence time within a network of reticulated reef ridges is on the order of tens of days (Andréfouët et al. 2001). Since water is highly incompressible, the flow velocity field can be specified by the stream function (ψ) (Eq. 5) that satisfies the mass continuity equation (Eq. 6) (Batchelor 2000);

$$u = \frac{\partial \psi}{\partial y} \text{ and } v = -\frac{\partial \psi}{\partial x} \tag{5}$$

$$\nabla(u, v) = \frac{\partial u}{\partial x} + \frac{\partial v}{\partial y} = \frac{\partial^2 \psi}{\partial x \partial y} - \frac{\partial^2 \psi}{\partial x \partial y} = 0 \tag{6}$$

where u and v are the components of flow velocity vector ($\vec{U}$) in the x and y directions, respectively.

Mixing-length theory (Duncan et al. 1960) links basal shear stress to hydrodynamic shear and flow velocities. Shear stress (τ) can be first estimated by an equivalent shear velocity (u_*) and fluid density (p, ton/m^3):

$$\tau = p{u_*}^2 \tag{7}$$

Within the turbulent boundary layer near the base of flow, a logarithmic decrease of flow velocity (U) with the height above seabed (z) is assumed, such that shear velocity can be related to the flow velocity by the "Law of the Wall" (Duncan et al. 1960) (Eq. 8).

$$\langle U \rangle = \frac{u_*}{k} \ln \frac{z}{z_0} \quad z_0 < z < z_b \tag{8}$$

where u_* is the shear velocity that scales with flow turbulence and affects reef growth rates (Eq. 2), k is von Karman's constant (0.407), z is the elevation of the seabed, z_b is the height of the boundary layer top, and z_0 is the roughness length that sets the elevation above the reefs at which flow velocity drops to zero. For coarse sediments and hydraulically rough flow, the roughness length is ~ 1/30 of the sediment grain size (Julien 2010). We assume a uniform sediment grain size of 2 mm, as is typical in reef systems (Purkis et al. 2014).

The average flow velocity over the boundary layer $\langle U \rangle$ can be calculated by integrating Eq. 8 between the roughness length (z_0) and the maximum height (z_b), assuming $z_b \gg z_0$:

$$\langle U \rangle = \left(\frac{u_*}{k}\right)\left(\ln\left(\frac{z_b}{z_0}\right) - 1 + \frac{z_0}{z_b}\right) \tag{9}$$

We further assume that steady-state flow moves around bathymetric highs and tends to minimize the total bed shear stress:

$$F = \int_0^x \int_0^y \tau \partial x \partial y \tag{10}$$

Combing Eqs. 5, 7, and 9, the shear stress (τ) in Eq. 10 can be replaced by Eq. 11 to derive the total bed shear stress (Eq. 12):

$$\tau = \frac{pk^2\left(\left(\frac{\partial \psi}{\partial x}\right)^2 + \left(\frac{\partial \psi}{\partial y}\right)^2\right)}{\left(ln\left(\frac{z_b}{z_0}\right) - 1 + \frac{z_0}{z_b}\right)^2} \tag{11}$$

$$F = \int_0^x \int_0^y f\left(\left(\frac{\partial \psi}{\partial x}\right)^2 + \left(\frac{\partial \psi}{\partial y}\right)^2\right) \mathrm{dxdy} \tag{12}$$

where f is defined as:

$$f = \frac{pk^2}{\left(ln\left(\frac{z_b}{z_0}\right) - 1 + \frac{z_0}{z_b}\right)^2} \tag{13}$$

The total bed shear stress can be minimized to solve for flow velocity (u and v) and shear velocity (u_*):

$$\frac{\partial}{\partial x}\left(f\frac{\partial \psi}{\partial x}\right) + \frac{\partial}{\partial y}\left(f\frac{\partial \psi}{\partial y}\right) = 0 \tag{14}$$

Initial conditions, boundary conditions, and model solution

Our model domain is 2 × 2 km and comprised of 100 × 100 cells, i.e., a grid cell is 20 × 20 m in size. Each time step in our model is one year, and a total of 5000-time steps gives a total elapsed model time (EMT) of 5000 years, a duration broadly in line with the ages of Holocene reticulated reefs, as supported by coring and geochronology studies (Delesalle 1985; Woodroffe et al. 1994; Wyrwoll et al. 2006; Purkis et al. 2008; 2010). We solve our model using a finite difference method.

The model is started with a random initial condition—100 reef pinnacles are randomly placed into the model domain (i.e., 1% cover). Each of these pinnacles has an initial biomass density (B) of 1 ton m^{-2}. At initiation, sediment (S) is absent in the model. Water depth (z) across the domain at initiation is 10 m, corresponding to the average depth of the lagoons at our 63 sites. For B, S and z, periodic boundary conditions were applied to the left and right boundaries of the model domain ($x=0$ and $x=100$), while Neumann boundary conditions were applied to the upper and lower boundaries ($y=0$ and $y=100$). Plausible model parameters were supported by literature (Table 1).

For the hydrodynamic flow module, an initial estimate of stream function (ψ) can be calculated for each grid cell depending on the input boundary flow direction (θ) and velocity (U_0). The total bed shear stress over the entire model surface can then be minimized by solving Eq. 14 using a numerical relaxation approach (Baker 2003), until the difference between successive iterations converges. Flow moves in the direction from the upper to lower boundary (set to be 0°) and the boundary flow velocity (U_0) is set to be 0.05 m s^{-1} (Delesalle 1985). The critical shear velocity (u_c) is set to be 0.01 m s^{-1}, assuming a uniform grain size of 2 mm (Miller et al. 1977).

Validation of the reef growth model with real-world reef maps

The 63 reef morphology examples mapped from PlanetScope satellite imagery serve as validation for the simulated reef morphologies generated by our reaction–diffusion model. As previously described, reef morphology at each of the 63 sites was quantified using three metrics—reef fraction, mean DCI, and characteristic wavenumber ($k1$). At 100-year time steps, we used the same three metrics to quantify our simulated reef morphologies.

We followed a three-step process to assess the model performance. Here, the three metrics that capture the patterning of the real-world reef: reef fraction, mean DCI, and $k1$ are denoted as (x, y, z). Those extracted from our simulations as $(\hat{x}, \hat{y}, \hat{z})$. In the first step, the total sum of squares (SST), which measures the total variance in the real-world observations, was calculated as follows:

$$\mathrm{SST} = \sum\nolimits_i \left(x_i - \bar{x}\right)^2 + \sum\nolimits_i \left(y_i - \bar{y}\right)^2 + \sum\nolimits_i \left(z_i - \bar{z}\right)^2 \quad (15)$$

(Eq. 15) where i is the site index, $\bar{x}$, $\bar{y}$, and $\bar{z}$ are the means of the real-world observations along each axis. Next, we calculated the values of these three spatial metrics for model-generated spatial patterns every 100-time steps (years). We then connected these values to construct a trajectory in a 3D space (this "trajectory" is similar to the regression line in linear regression models in a 2D space). For (x_i, y_i, z_i) associated with site i, it is projected to the constructed trajectory to identify the point on the constructed trajectory that is closest to (x_i, y_i, z_i). We identified that point as the model-predicted values of the three spatial metrics for the site i, that is, $(\hat{x}_i, \hat{y}_i, \hat{z}_i)$. Next, the residual sum of squares (RSS) was calculated:

$$\mathrm{RSS} = \sum\nolimits_i \left(x_i - \hat{x}_i\right)^2 + \sum\nolimits_i \left(y_i - \hat{y}_i\right)^2 + \sum\nolimits_i \left(z_i - \hat{z}_i\right)^2 \quad (16)$$

Table 1 Summary of model parameters, including definitions, units, values used in this study, and supporting literature

Variable	Description	Unit	Value	Source	Notes
r	Maximum Holocene coral reef growth rate	Ton $year^{-1}$ m^{-2}	0.08	Enos (1991) and Dullo (2005)	Note this is the potential maximum growth rate, not the actual accretion rate
k_s	Water depth at which reef growth is half maximum	m	5.00	Estimated	Estimated from the relationship in Bosence and Waltham (1990)
m	Mortality rate	1 $year^{-1}$	0.01	Estimated	N.A
D_1	Diffusion coefficient of coral reef expansion	m^2 $year^{-1}$	0.02	Calibrated	Estimated from a lateral reef accretion rate of 9 cm $year^{-1}$ (Kennedy and Woodroffe 2002; Yamano et al. 2003), using the approach of Cain (1990)
c	Conversion constant of dead reef to transported sediment	m^3 t^{-1}	0.30	Masiero et al. (2020)	Down-slope transport of sediment debris
D_2	Diffusion coefficient of sediment transport	m^2 $year^{-1}$	1.00	Burgess and Steel (2008), Simon et al. (2022)	Marine sand can be as low as 0.1 m^2 $year^{-1}$
γ	Bulk density of reef framework	Ton m^{-2}	1.60	Buddemeier et al. (1974), Hopley (2011)	Bulk density ranges from 1 to 2.2 g cm^{-3}

Table 2 Comparison of real-world reef patterns with those modeled using unidirectional, variable, and random hydrodynamic flow regimes

Simulated flow regime	Total sum of squares (SST)	Residual sum of squares (RSS)	Coefficients of determination (R^2)
Unidirectional	8.59	1.42	0.83
Variable	8.52	1.21	0.86
Random	8.89	1.69	0.81

Coefficients of determination (R^2) for all three regimes are > 0.8

Finally, the coefficient of determination (R^2) for each model run was calculated:

$$R^2 = 1 - \frac{\mathrm{RSS}}{\mathrm{SST}} \tag{17}$$

Values for SST, RSS, and R^2 for our simulations are presented in Table 2.

Results

Clustering real-world reef patterns

Clustering of the binary representations of the 63 real-world sites suggests the reef patterning to split into seven classes within the three-parameter space of the pattern's characteristic wavenumbers ($k1$), mean directional connectivity index (DCI), and proportional fraction of reef ridges (Fig. 4).

Across these seven classes, there is a progressive increase in reef fraction and mean DCI, accompanied by a consistent decline in $k1$ (Fig. 4). These trends suggest a systematic trajectory of reef pattern development, as individual patch reefs coalesce to form dense reef networks. This development neatly follows the seven-class trajectory in reef patterns suggested by statistical clustering of the 63 real-world sites. Starting as small isolated patch reefs in the lagoon (Fig. 4, Class 1), lateral reef expansion increases individual patch size (Classes 2 and 3), followed by the development of elongated reef shapes which in turn develop into incipient ridges (Class 4).

Continued lateral expansion and coalescence between adjacent reefs serve to further increase both reef fraction and connectivity (Class 5), ultimately creating highly interconnected polygonal reef networks (Class 6). Classes 5 and 6 are differentiated by the presence of isolated patch reefs in Class 5, which are absent in Class 6. By the time that the reefscape has evolved to Class 6, the reef ridges are sufficiently developed to encircle portions of the lagoon floor, forming "ponds".

Sites at the terminal phase of development, Class 7, form well-connected networks of reef ridges characterized by the highest reef fraction and DCI values. Several sites classified as Class 7 show two spatial scales of reef patterning—small ponds encircled by thin ridges contained within larger ponds with thicker ridges—as identified in Modern Alacranes Reef and in reefs built by now-extinct calcareous

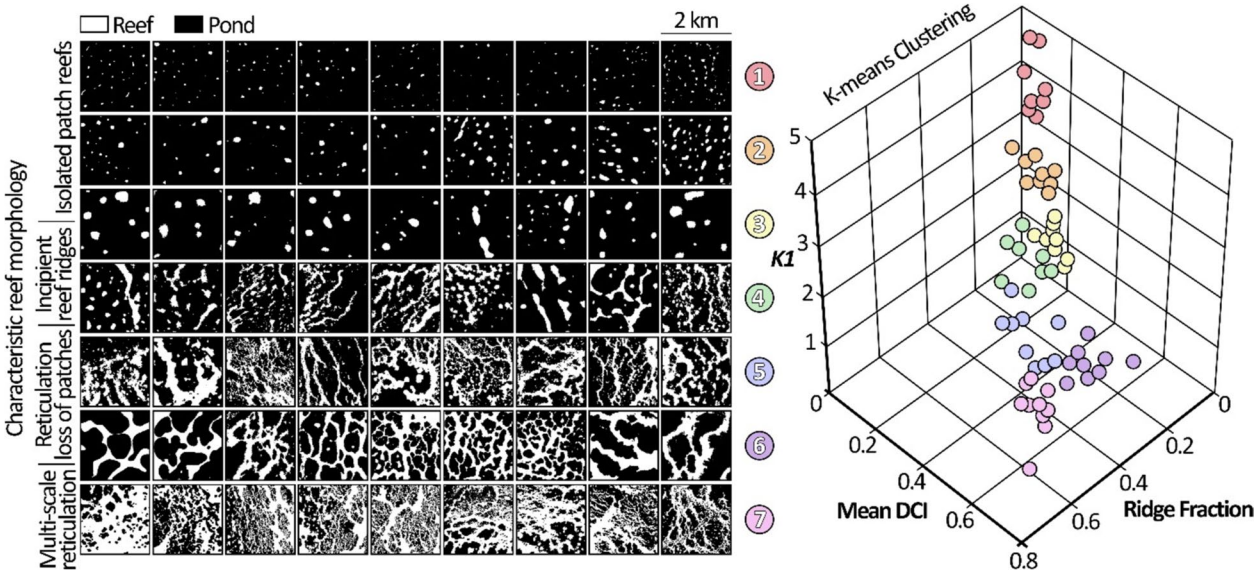

Fig. 4 Clustering of reef morphologies mapped at 63 global reef sites. Using a *K*-means classifier, the morphologies logically split into seven classes based on their characteristic wavenumbers ($k\ 1$), mean directional connectivity index (DCI), and proportional fraction of reef ridges in each 2 × 2 km mapped area

algae 300 million years ago by Purkis et al. (2015)—their Fig. 14

Numerical simulation of patterned reef development

The synthetic reefs produced by our reaction–diffusion model develop along a trajectory composed of four distinct stages, with the first being the random initiation of the simulation with 100 reef pinnacles within the 2 × 2 km model domain. In the second stage, those pinnacles coalesce into incipient reef ridges, which in turn produce semi-enclosed inter-ridge ponds (the third stage). In the model's fourth and final stage, dense reticulated reef ridges emerge with fully enclosed ponds.

As developed in Fig. 5, the evolution of the modeled reefs can further be examined in the context of their growth dynamics. In the first 1000 years of elapsed model time (EMT), the simulated reefs primarily aggrade vertically. Sediment shed by these growing reef pinnacles accumulates in their vicinity on the seabed. Despite some small variations in hydrodynamic shear velocity around the pinnacles, the overall velocity distribution remains homogeneous within the model domain during this development phase.

By EMT = 2000 years, most reefs approach the sea surface, prompting a switch in their growth mode from vertical accretion to lateral progradation. Hydrodynamic shear velocity starts to elevate around the flanks of the simulated pinnacles, further promoting reef lateral growth. Continued reef progradation and sediment shedding fills the intervening space between adjacent pinnacles, thereby facilitating the lateral coalescence of the reefs into low-relief (incipient) ridges, which orientate perpendicular to the flow direction.

By EMT = 3000 years, the incipient reef ridges span the model domain and fully aggrade to the sea surface,

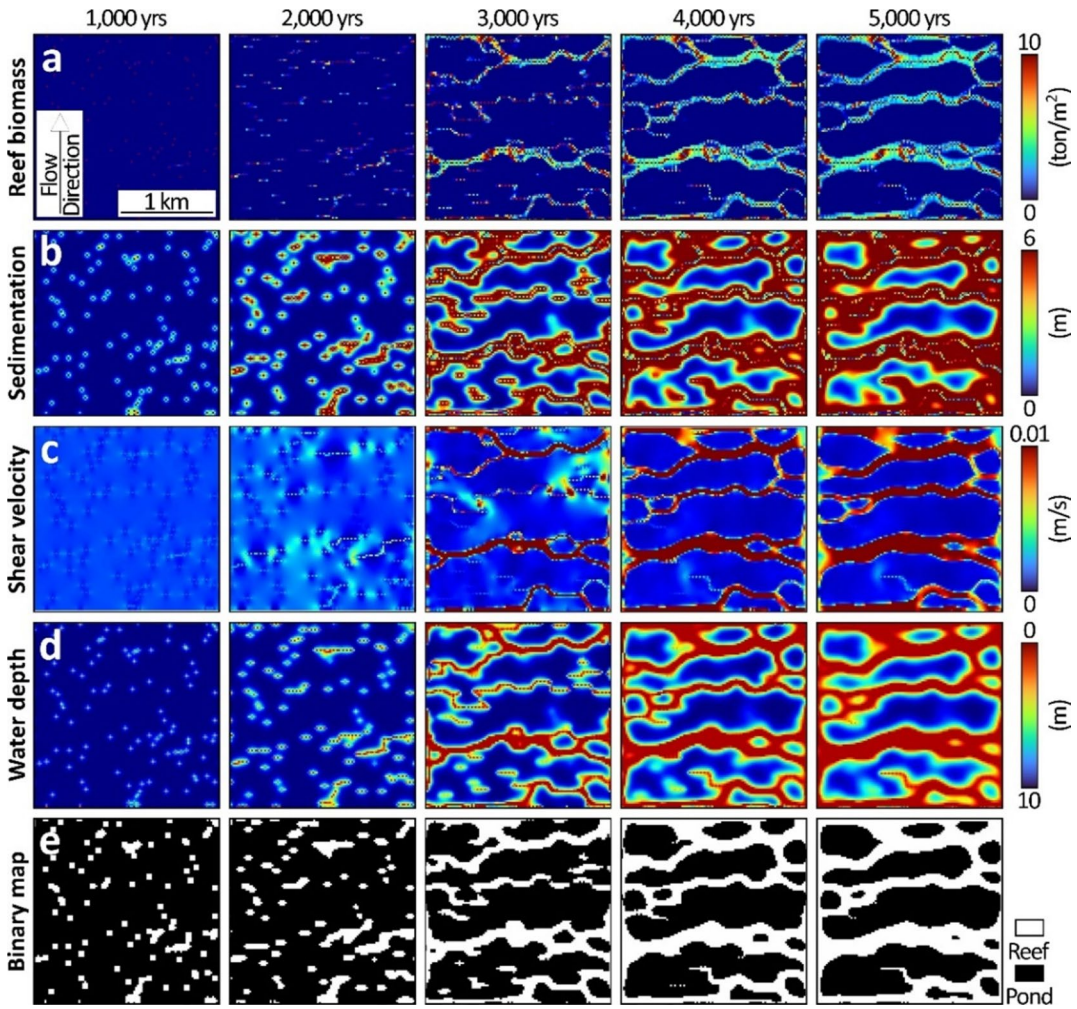

Fig. 5 Evolution of the reef morphogenesis over 5000 years of elapsed model time (EMT) under a unidirectional flow regime. At 1000-year increments, tracked in (**a**) is reef biomass, sediment accumulation (**b**), hydrodynamic shear velocity (**c**), water depth (**d**), and a binary representation of the model in terms of reefs and ponds (**e**). Note how reticulate reef patterns emerge after 3000 model years

promoting lateral progradation. The now well-developed ridges baffle hydrodynamic flow, greatly reducing shear velocity in their lees.

By EMT = 4000 years, further reef coalescence starts to bridge the deep water separating the ridges. With the formation of these bridges, ponds emerge in the simulation. Sheltered by competent rings of reef ridges, shear velocity in the ponds drops to near zero. By this stage in the simulation, the modeled bathymetry predominantly evolves due to gradual infilling of the lagoon floor by sediments shed from the now densely packed network of reef ridges. Simulation beyond 4000 years yields little change of reef morphology as the model has reached a dynamic equilibrium state. The production of reef biomass plateaus (Fig. 6a) and hydrodynamic equilibrium is attained across the model domain (Fig. 6b).

Effects of flow direction on reef patterning

Given that it takes 4000 years for our model to reach equilibrium, it is reasonable to assume that the direction of hydrodynamic flow in a real-world scenario would not remain constant over such an extended period. Even on short timescales, for instance, the currents that sweep coral reefs can change seasonally, as assessed by Rankey (2021) in the South China Sea and Lopez-Gamundi et al. (2022) in the Bahamas. We therefore examined the effect of variable flow directions on the reef morphologies. To do so, we altered its boundary flow direction (θ) to conduct three numerical experiments.

In the first experiment, we set the boundary conditions such that hydrodynamic flow direction (θ) in the model constant over the 5000-year simulation ($\theta = 0°$), i.e., "unidirectional flow" scenario. In the second, flow direction

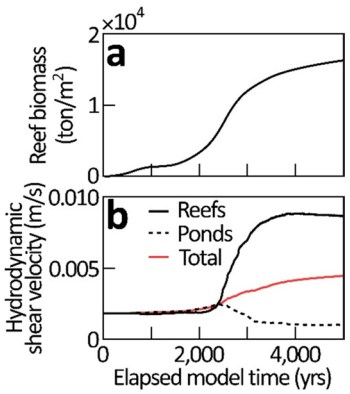

Fig. 6 Evolution of reef biomass and hydrodynamic shear velocity over 5000 years of simulation. Biomass (**a**) rapidly increases between 2000 and 4000 years, as reticular reef ridges develop (Fig. 5). In **b**, shear velocity is averaged over the cells in the simulation containing reefs ("Reefs"), those containing "Ponds", and over the entire model domain ("Total")

was varied randomly between $\theta = -90°$ and 90° (random flow scenario) and in the last experiment, θ was varied with every 1000 years between − 30 and 30°, i.e., variable flow scenario, as portrayed in Fig. 7a.

Clear from these three experiments is that modeled flow direction has only a weak effect at the early stage (< 1000 years) when the reefs are in their pinnacle phase (Fig. 7b). After 1000 years, however, the reef morphologies delivered by the three flow regimes diverge, becoming visually distinct by EMT = 3000 years. By that time, the reef ridges generated under unidirectional flow orientate normal to flow direction—the reef pattern is anisotropic. By contrast, the ridges in the random flow direction after 3000 years of simulation have no preferential orientation, and the emergent patterns are reticulated and isotropic. Note too that the ponds produced under random flow are smaller and more completely enclosed than patterns formed under the other flow scenarios. Finally, the ridges formed in the variable flow experiment split the difference between those produced in the unidirectional and random regimes. Here, the reef ridges display weak preferential orientation (anisotropy).

We further quantified the differences in the reef spatial patterns formed in the three flow regimes using the four pattern metrics described previously—reef fraction, directional connectivity index (DCI), characteristic wavenumber ($k1$), and principal axis ratio (PAR). For each flow regime, we repeated the simulations 100 times with different random initial conditions (i.e., random configuration of pinnacle reefs) to construct the mean and variance of each spatial metric every 100-year time step (Fig. 8).

For all three flow regimes, reef fraction and mean DCI increase over time (Fig. 8a, b) while $k1$ decreases (Fig. 8c). It is in the PAR metric, which captures the degree of isotropy/anisotropy of the reef patterns, that the three simulated flow regimes diverge (Fig. 8d). PAR for the reefs building under unidirectional and variable flow start to rise after 1500 years. This inflection in PAR corresponds to the appearance of the first reef ridges under these flow regimes at that time (Fig. 7). The timing of peak PAR—a proxy for the emergence of interconnected reef ridges (surrounding enclosed ponds)—differs between the flow regimes (Fig. 8d). The PAR curve for unidirectional flow peaks at 2500 years, under variable flow regime at 2700 years, and at 3000 years for the random flow regime. These results suggest that shifts in current direction might delay the emergence of reef patterns. Furthermore, PAR is significantly higher for patterns formed in unidirectional flows than those formed in random flow regime (Fig. 8d), confirming results from our visual inspections of the patterns (Fig. 7). In the variable flow regime, PAR is at the intermediate level.

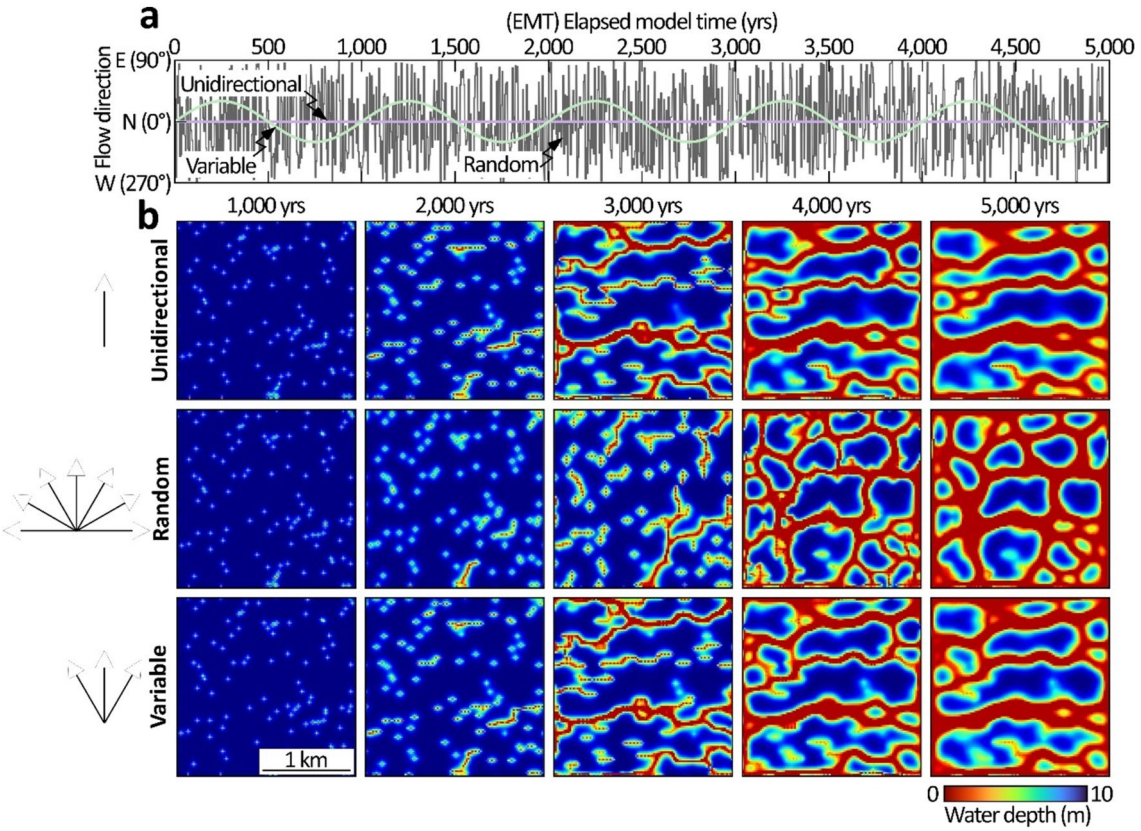

Fig. 7 Evolution of simulated bathymetry under three regimes of hydrodynamic flow. **a** Over three 5000-year model runs, flow was set to either unidirectional, random, or variable, through which reef development was tracked (**b**). Note how the simulations run under unidirectional and variable flow are anisotropic, since the reefs develop perpendicular to flow direction. Random flow, by contrast, lacking a preferred direction, delivers isotropic (honeycomb-like) reef patterns

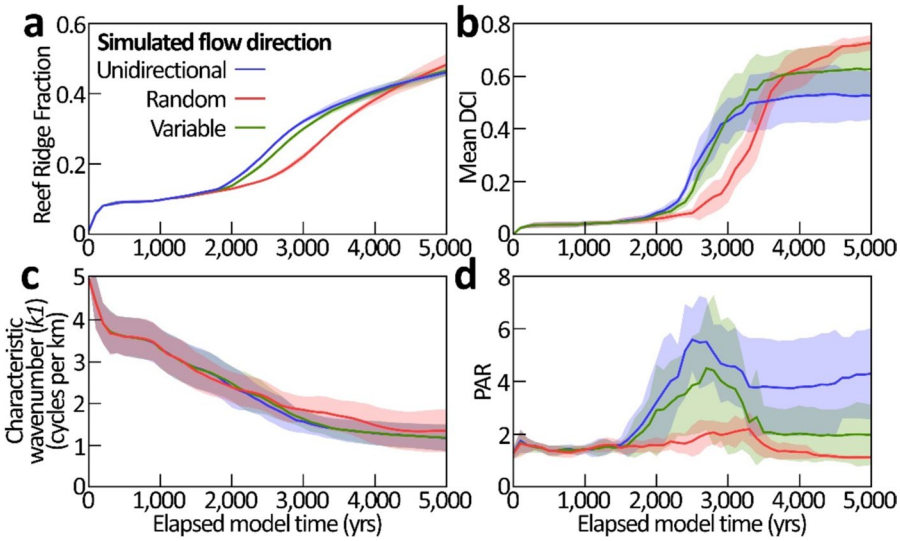

Fig. 8 Evolution of the morphology of simulated reefs over 5000-year model runs using unidirectional, random, and variable hydrodynamic flow regimes. Morphology quantified using reef fraction (**a**), mean directional connectivity index (DCI) (**b**), characteristic wavenumber (*k1*) (**c**), and principal axis ratio (PAR) (**d**). Envelopes represent 95% confidence intervals around each pattern metric

Reaction–diffusion modeling reproduces real-world reef patterns

We adopted two strategies to evaluate whether our model can reproduce the observed reef patterns at the 63 real-world sites which we mapped from satellite. The first of those strategies was qualitative. We plotted the observed and modeled patterns in the now familiar three-axis data-space of reef fraction, mean DCI, and *k1* (Fig. 9). For the simulated reefs, we extracted these three pattern metrics from the model at 100-year increments for the duration of each run. This process was conducted for the models run with each of the three flow regimes (unidirectional—Fig. 9a, variable—Fig. 9b, and random—Fig. 9c). Each regime was run five times, using different random initial conditions, yielding 15 model trajectories in total.

Comparing the reef patterns mapped at the 63 sites with these 15 simulated trajectories reveals the model to be broadly capable of reproducing the real-world patterns and their evolution, especially for incipient reef ridges (Class 4) and dense reticulated ridges (Class 5, 6, and 7) (Fig. 9).

Next to quantify the capacity of the models reproduce the real-world patterns, we calculated the coefficient of determination (R^2) from the three patterns metrics. The results show $R^2 > 0.8$ for all three flow regimes, suggesting a satisfactory fit between observations and model predictions (Table 2). There are, however, caveats to the model performance. It lacks skill in reproducing large, isolated patch reefs, such as those in Class 3 (Fig. 4). However, the overall model goodness-of-fit suggests that reticulated reef patterns can emerge from simple random initial conditions by spatial self-organization.

Discussion

Reticulate reef patterning is a broad-scale response to prevailing environment

This study builds on a growing body of work on reefs which display coherent patterns. Using a Turing-type reaction–diffusion model, validated by real-world reef maps, we provide a mechanistic understanding of the ecosystem feedbacks which conspire to deliver emergent reef patterning. Albeit with a complex mathematical formulation, our model captures a relatively narrow suite of parameters pertaining to reef development. For instance, guided by literature, we parameterize the assumed relationships which relate hydrodynamic flow and water depth to reef growth. We also presume to capture realistic rates of reef mortality and sediment production. Much is left out of the model. For instance, the competition for space between juvenile corals and algae, intermittent crises as wrought by bleaching, predator outbreaks, coral diseases, and so on. Nor do we simulate the changing carbonate saturation state of the waters

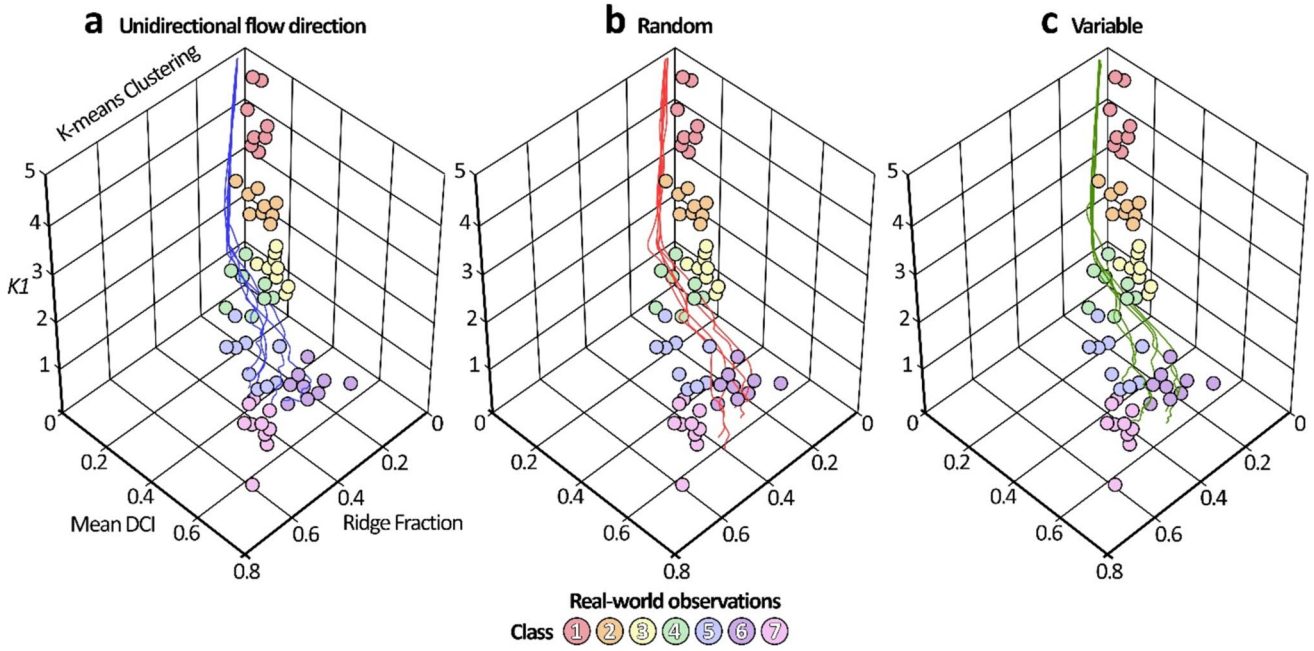

Fig. 9 Comparison of real-world reef patterns with those delivered using simulation under three regimes of hydrodynamic flow—unidirectional (**a**), random (**b**), and variable (**c**). For all three regimes, the simulated reef patterns track those mapped from satellite, as quantified using *k*1, mean DCI, and reef ridge fraction, emphasizing the capability of the model to mimic real-world morphologies

surrounding the reefs, their oxygen content, or alkalinity. In fact, we consciously elected to minimize the quantity of variables in our model. Doing so shortens its causal chains, making results easier to interpret.

Yet, even with a simplified representation of reef function, our simulations follow a similar trajectory of morphogenesis as displayed by real-world reefs (Figs. 7 and 9). Too, our simulation yields reef patterns which are statistically similar to those mapped from the real world (Table 2). Is this success a surprise? Perhaps not, if pattern formation is a high-level generalized response of the reef architect to its surrounding environment. Insight into this generality can be gleaned from the behavior of modern and ancient reefs, including those built by organisms other than corals.

First, let us examine the notion that pattern formation is a high-level response, not predicated, for instance, on the species of corals that construct the reef. Certainly, reticulated reefs equally grow in the Arabian Gulf (Purkis et al. 2010) and tropical Atlantic (Zlatarski and Greenstein 2020) where the diversity of coral species is low, as in the tropical Pacific (Schlager and Purkis 2015) and Great Barrier Reef (Blakeway and Hamblin 2015; Blakeway 2018), where it is high. The morphogenic behavior is evidently not an ecological nuance restricted to a certain coral assemblage or locality. Next consider that reticulate patterns are not even specific to reefs built by corals. The vast *Halimeda* (a calcareous macroalgae) reefs of the Great Barrier Reef reticulate (McNeil et al. 2021), as do the microbially-precipitated stromatolites in Shark Bay (Suosaari et al. 2019; Xi et al. 2022), also in Australia. Then, consider Purkis et al. (2015) who show how *Palaeoaplysina* (an extinct phylloid algae) built reticulate reefs 300 million years ago. The authors of that study demonstrate how the patterns of the ancient algal reefs are morphologically inseparable to those constructed by modern corals. Precambrian stromatolites, some of Earth's earliest lifeforms, likely patterned similarly (van de Vijsel et al. 2020). All these studies advocate morphogenesis to be a high-level response of the reef builder to its surrounding environment, but how is reticulate patterning triggered?

Hydrodynamic restriction proceeds reef reticulation

We attribute reef pattern emergence to strong couplings between coral growth and hydrodynamic flow. Blakeway and Hamblin (2015), by contrast, linked pattern emergence to episodic collapse of *Acropora*-dominated coral frameworks driven by gravity. Blakeway (2018) later refined this "collapse" model, suggesting that hypoxia from water-mass stagnation in inter-ridge ponds inhibits reef growth, reinforcing the formation of "cells" in the reef framework. The Blakeway hypothesis is interesting given more recent work which shows how swiftly oxygen can become depleted in a restricted reef environment and how susceptible corals are to even brief episodes of hypoxia (Swaminathan et al. 2024). The Blakeway (2018) hypoxia model generally aligns with our own understanding of emergent reef patterning, though we attribute is trigger to be reduced hydrodynamic flow in inter-ridge ponds, rather than specifically to oxygen depletion. Both models share broad similarities, though ours employs differential equations rather than cellular automata. Notably, reticulated reef patterns emerge within 2000–4000 years in Blakeway's simulations, matching our model's timing (Fig. 7).

The reef ridges in our simulation begin to reticulate when the water mass surrounding them becomes restricted. Note the drastic drop in hydrodynamic shear velocity in the simulation as the pattern emerges (Fig. 5). As reviewed by Schutter et al. (2010), vigorous hydrodynamic flow is important to the coral organism for both photosynthesis and for respiration. Feeding efficiency, dissolved gas, nutrient, and inorganic carbon uptake all increase as a function of increasing flow. As flow nourishes the coral's physiology, it is also important for removal of harmful metabolites (Nakamura and van Woesik 2001), removal of nuisance sediment, cyanobacteria, and the algae which might otherwise suffocate the coral (Rogers 1990; Anthony and Fabricius 2000; Box and Mumby 2007). For all these reasons, coral growth rate displays a positive correlation with hydrodynamic flow (Schutter et al. 2010), at least up until the point that flow becomes so brisk as to be physically damaging (Sebens 1997), but such strong currents are not encountered under prevailing conditions in sheltered lagoons, and hence represent an edge case to this study. Neither is the importance of flow restricted to shallow-water reefs. Deep-water corals similarly benefit from it (Correa et al. 2012; van der Kaaden et al. 2021).

With hydrodynamic flow exerting sway over so many aspects of coral physiology, it is logical to examine how it might be connected to coherent reef patterning. Indeed, flow was central to the hypothesis put forward by Purkis et al. (2016) and is implicated via hypoxia in the one proposed by Blakeway (2018).

Reef morphogenesis triggered by scale-dependent feedbacks

Work beyond reefs elegantly shows how scale-dependent feedbacks are common triggers for emergent patterning through self-organization. One of the classic examples comes from dryland vegetation (van de Koppel et al. 1997; 2002; Rietkerk et al. 2002). Here, positive feedbacks at short distances, such as increased infiltration and soil moisture retention under vegetation patches, are countered by negative feedbacks at larger scales, like reduced water availability between patches. The interaction of these feedbacks, offset

in scale, triggers emergent patterning, with the long-range negative feedback primarily driving pattern formation, and the short-range activation serving to "sharpen" it (van de Koppel and Crain 2006; Rietkerk and van de Koppel 2008). Reticulate patterns in terrestrial systems delivered by these mechanisms are striking similar to those built by reefs, as recognized by Rietkerk and van de Koppel (2008).

Our models show a possible pathway whereby feedbacks between hydrodynamic flow and reef growth trigger morphogenesis. At the early stage of seabed colonization, patch reefs growing in favorable conditions start to expand to form ridges. The currents that flow across this hydrodynamically unrestricted seabed impart kinetic energy onto the surface relief of those ridges, inducing turbulence. The corals inhabiting the ridges grow swiftly in these advantageous conditions, by virtue of their enhanced uptake of dissolved gasses, nutrients, and inorganic carbon in turbulent flow. The coral's harmful metabolites are efficiently shed. Plenty of the organism's energy is available for reproduction, creating many juvenile corals, which easily find excellent settlement substratum nearby, swept clear of sediment. The coral assemblage thrives, and the ridges grow vertically to sea level. We consider this sequence to represent a positive ("activation") feedback operating at a short length scale.

Once the reef ridges reach sea level, their growth modality switches to lateral extension. The ridges broaden, restricting the water mass separating them. This water mass stagnates as hydrodynamic flow diminishes toward zero (Figs. 5 and 6). Reduced turbulence hampers all aspects of the coral's physiology. Growth rate accordingly slows, and the sediment produced by the reef accumulates on the flanks of the ridges. This growing sediment apron imposed a long-range negative ("inhibitive") feedback on the system. The interaction of the short-range activation feedback and the long-range inhibition induces the emergence of coherent pattern. To the advantage of the overall reef system, the reticulated pattern of reef ridges maximizes the ratio of reef coverage to open water that can be accommodated in the finite size of the increasingly sediment-filled lagoon.

Conclusions and implications

Our study suggests spatial self-organization, rooted in complex feedbacks between sedimentation, flow dynamics, and coral growth, as the underlying mechanism giving rise to the reticulate reef patterns. Results from our numerical model suggest that patterned reef ridges develop as a result of the metabolic stress induced in corals inhabiting a stagnated water mass. If morphogenesis is triggered by water-mass stagnation, reticulate patterns appearing at scales from hundreds of meters to kilometers can help us understand ecosystem stress impacting corals at the scale of individual colonies. Thus, using satellite sensing, the scaling laws of life could be employed as a global-scale monitoring tool for assessing reef health. We suggest that emergent patterning through spatial self-organization will become a promising area of research in coral reef science.

Acknowledgements We thank Ana Tarano for advice on image processing, Estanislao Kozlowski for help with hydrodynamic modeling, and Peter Burgess for mentorship. We are grateful for the critique of two anonymous reviewers. Their comments enhanced the quality of this paper. Xi, Chirayath, Gleason, and Purkis were funded by NASA ROSES Biodiversity Award 20-BIODIV20-0108 (MarineVERSE). Dong was funded by National Science Foundation grant OPP #2333917. PlanetScope satellite imagery provided by Chirayath through the NASA CSDA Program, Planet Team (2023, 2024). Planet Application Program Interface: In Space for Life on Earth. San Francisco, CA.

Declarations

Conflict of interest On behalf of all authors, the corresponding author states that there is no conflict of interest.

References

Andréfouët S, Pagès J, Tartinville B (2001) Water renewal time for classification of atoll lagoons in the Tuamotu Archipelago (French Polynesia). Coral Reefs 20:399–408

Anthony KR, Fabricius KE (2000) Shifting roles of heterotrophy and autotrophy in coral energetics under varying turbidity. J Exp Mar Biol Ecol 252(2):221–253

Aronson RBWF, Precht W, Toscano M, Koltes KH (2002) The 1998 bleaching event and its aftermath on a coral reef in Belize. Mar Biol 141:435–447

Atkinson M, Falter J, Hearn C (2001) Nutrient dynamics in the biosphere 2 coral reef mesocosm: water velocity controls NH_4 and PO_4 uptake. Coral Reefs 20:341–346

Baker Y (2003) Development of a three-dimensional shallow marine suspended sediment distribution model (SUSD3D) with application to the coarse-grained deltas of the intracontinental strike-slip Bohemian Cretaceous basin. In: Doctoral dissertation, Royal Holloway, University of London

Bastiaansen R, Jaïbi O, Deblauwe V, Eppinga MB, Siteur K, Siero E, Mermoz S, Bouvet A, Doelman A, Rietkerk M (2018) Multistability of model and real dryland ecosystems through spatial self-organization. Proc Natl Acad Sci 115(44):11256–11261

Batchelor GK (2000) An introduction to fluid dynamics. Cambridge University Press

Blakeway D (2018) Hypoxia shapes coral reefs. PeerJ Preprints 6:e26794v1

Blakeway D, Hamblin MG (2015) Self-Generated Morphology in Lagoon Reefs. PeerJ 3:e935

Bosence D, Waltham D (1990) Computer modeling the internal architecture of carbonate platforms. Geology 18(1):26–30

Box SJ, Mumby PJ (2007) Effect of macroalgal competition on growth and survival of juvenile Caribbean corals. Mar Ecol Prog Ser 342:139–149

Budd DA, Hajek EA, Purkis SJ (2016) Introduction to autogenic dynamics and self-organization in sedimentary systems. SEPM Spec Publ 106:1–4

Buddemeier RW, Maragos JE, Knutson DW (1974) Radiographic studies of reef coral exoskeletons: rates and patterns of coral growth. J Exp Mar Biol Ecol 14(2):179–199

Burgess PM, Steel RJ (2008) Stratigraphic forward modeling of basin-margin clinoform systems: implications for controls on topset and shelf width and timing of formation of shelf-edge deltas. Recent advances in models of siliciclastic shallow-marine stratigraphy. SEPM Society for Sedimentary Geology

Cain ML (1990) Models of clonal growth in *Solidago altissima*. J Ecol 78:27–46

Chirayath V, Bagshaw E, Craft K, Dierssen H, Lim D, Malaska M, Pizarro O, Purkis S, Schroeder D, Sobron P, Waller S (2022) Oceans across the solar system and the search for extraoceanic life. Oceanography 35(1):54–65

Coco G, Murray AB (2007) Patterns in the sand: from forcing templates to self-organization. Geomorphology 91(3–4):271–290

Correa TB, Grasmueck M, Eberli GP, Reed JK, Verwer K, Purkis SAM (2012) Variability of cold-water coral mounds in a high sediment input and tidal current regime, Straits of Florida. Sedimentology 59(4):1278–1304

Couteron P, Lejeune O (2001) Periodic spotted patterns in semi-arid vegetation explained by a propagation-inhibition model. J Ecol 89(4):616–628

Dee S, Zweifler A, Cuttler M, Nilsen J, Bonesso J, O'Leary M, Browne NK (2024) The application of carbonate and sediment budgets to assess the stability of marginal reef systems. Mar Geol 473:107324

Delesalle B (1985) Environmental survey of Mataiva Atoll, Tuamtu Archipelago, French Polynesia. Atoll Res Bull 286:1–34

Dong X, Murray AB, Heffernan JB (2021) Competition among limestone depressions leads to self-organized regular patterning on a flat landscape. J Geophys Res Earth Surf 126(5):e2021JF006072

Dullo WC (2005) Coral growth and reef growth: a brief review. Facies 51(1):33–48

Duncan WJ (1960) An elementary treatise on the mechanics of fluids. University of Glasgow, Scotland, Edward Arnold Publishers Ltd., London, Printed in Northern Ireland at the University Press, Belfast

Eddy TD, Lam VW, Reygondeau G, Cisneros-Montemayor AM, Greer K, Palomares MLD, Bruno JF, Ota Y, Cheung WW (2021) Global decline in capacity of coral reefs to provide ecosystem services. One Earth 4(9):1278–1285

Enos P (1991) Sedimentary parameters for computer modeling. Bulletin (Kansas Geological Survey) 233:63–99

Gardner TA, Côté IM, Gill JA, Grant A, Watkinson AR (2003) Long-term region-wide declines in Caribbean corals. Science 301(5635):958–960

Génin A, Navarrete SA, Garcia-Mayor A, Wieters EA (2024) Emergent spatial patterns can indicate upcoming regime shifts in a realistic model of coral community. Am Nat 203(2):204–218

Guilcher A (1988) Coral reef geomorphology

Hearn C, Atkinson M, Falter J (2001) A physical derivation of nutrient-uptake rates in coral reefs: effects of roughness and waves. Coral Reefs 20:347–356

Helmuth BS, Sebens KP, Daniel TL (1997) Morphological variation in coral aggregations: branch spacing and mass flux to coral tissues. J Exp Mar Biol Ecol 209(1–2):233–259

Holmes EE, Lewis MA, Banks JE, Veit RR (1994) Partial differential equations in ecology: spatial interactions and population dynamics. Ecology 75(1):17–29

Hopley D (1982) The geomorphology of the Great Barrier Reef. Wiley, New York, p 453

Hopley D (2011) Density and porosity: influence on reef accretion rates. Springer, Dordrecht

Hughes TP, Anderson KD, Connolly SR, Heron SF, Kerry JT, Lough JM, Baird AH, Baum JK, Berumen ML, Bridge TC, Claar DC (2018) Spatial and temporal patterns of mass bleaching of corals in the Anthropocene. Science 359(6371):80–83

Julien PY (2010) Erosion and sedimentation. Cambridge University Press

Kennedy DM, Woodroffe CD (2002) Fringing reef growth and morphology: a review. Earth Sci Rev 57(3–4):255–277

Kerr JM, Purkis S (2018) An algorithm for optically-deriving water depth from multispectral imagery in coral reef landscapes in the absence of ground-truth data. Remote Sens Environ 210:307–324

Larsen LG, Choi J, Nungesser MK, Harvey JW (2012) Directional connectivity in hydrology and ecology. Ecol Appl 22(8):2204–2220

Liu QX, Herman PM, Mooij WM, Huisman J, Scheffer M, Olff H, Van De Koppel J (2014) Pattern formation at multiple spatial scales drives the resilience of mussel bed ecosystems. Nat Commun 5(1):5234

Lopez-Gamundi C, Dobbelaere T, Hanert E, Harris PM, Eberli G, Purkis SJ (2022) Simulating sedimentation on the Great Bahama Bank-Sources, sinks and storms. Sedimentology 69(7):2693–2714

MacQueen J (1967) Some methods for classification and analysis of multivariate observations. In: Proceedings of the fifth Berkeley symposium on mathematical statistics and probability, vol 1, no 14, pp 281–297

Marshall JF, Davies PJ (1982) Internal structure and Holocene evolution of one tree reef, southern Great Barrier Reef. Coral Reefs 1:21–28

Masiero I, Kozlowski E, Antonatos G, Xi H, Burgess P (2020) Numerical stratigraphic forward models as conceptual knowledge repositories and experimental tools: an example using a new enhanced version of CarboCAT. Comput Geosci 138:104453

McNeil MA, Nothdurft LD, Dyriw NJ, Webster JM, Beaman RJ (2021) Morphotype differentiation in the Great Barrier Reef *Halimeda* bioherm carbonate factory: internal architecture and surface geomorphometrics. The Depositional Record 7(2):176–199

Miller MC, McCave IN, Komar P (1977) Threshold of sediment motion under unidirectional currents. Sedimentology 24(4):507–527

Mistr S, Bercovici D (2003) A theoretical model of pattern formation in coral reefs. Ecosystems 6:0061–0074

Nakamura TV, Van Woesik R (2001) Water-flow rates and passive diffusion partially explain differential survival of corals during the 1998 bleaching event. Mar Ecol Prog Ser 212:301–304

Perry CT, Spencer T, Kench PS (2008) Carbonate budgets and reef production states: a geomorphic perspective on the ecological phase-shift concept. Coral Reefs 27:853–866

Petroff AP, Wu TD, Liang B, Mui J, Guerquin-Kern JL, Vali H, Rothman DH, Bosak T (2011) Reaction–diffusion model of nutrient uptake in a biofilm: theory and experiment. J Theor Biol 289:90–95

Purdy EG (1974) Reef configurations: cause and effect. Reefs in time and space. Society of Economic Palaeontologists and Mineralogists. Spec Publ 18:9–76

Purdy EG, Bertram GT (1993) Carbonate concepts from the Maldives, Indian Ocean. American Association of Petroleum Geologists

Purkis SJ, Kohler KE (2008) The role of topography in promoting fractal patchiness in a carbonate shelf landscape. Coral Reefs 27:977–989

Purkis SJ, Riegl B (2005) Spatial and temporal dynamics of Arabian Gulf coral assemblages quantified from remote-sensing and *in situ* monitoring data. Mar Ecol Prog Ser 287:99–113

Purkis SJ, Kohler KE, Riegl BM, Rohmann SO (2007) The statistics of natural shapes in modern coral reef landscapes. J Geol 115(5):493–508

Purkis SJ, Rowlands GP, Riegl BM, Renaud PG (2010) The paradox of tropical karst morphology in the coral reefs of the arid Middle East. Geology 38(3):227–230

Purkis S, Kerr J, Dempsey A, Calhoun A, Metsamaa L, Riegl B, Kourafalou V, Bruckner A, Renaud P (2014) Large-scale carbonate platform development of Cay Sal Bank, Bahamas, and implications for associated reef geomorphology. Geomorphology 222:25–38

Purkis S, Casini G, Hunt D, Colpaert A (2015) Morphometric patterns in Modern carbonate platforms can be applied to the ancient rock record: similarities between Modern Alacranes Reef and Upper Palaeozoic platforms of the Barents Sea. Sed Geol 321:49–69

Purkis SJ, Gleason AC, Purkis CR, Dempsey AC, Renaud PG, Faisal M, Saul S, Kerr JM (2019) High-resolution habitat and bathymetry maps for 65,000 sq. km of Earth's remotest coral reefs. Coral Reefs 38:467–488

Purkis SJ, van de Koppel J, Burgess PM (2016) Spatial self-organization in carbonate depositional environments. SEPM Society for Sedimentary Geology Special Publication 106:53–66

Quintero CJ, Cohen MJ (2019) Scale-dependent patterning of wetland depressions in a low-relief karst landscape. J Geophys Res Earth Surf 124(8):2101–2117

Rankey EC (2021) Platform-top reef sand apron morphodynamics and the half-empty bucket. Sed Geol 412:105825

Renshaw E, Ford ED (1984) The description of spatial pattern using two-dimensional spectral analysis. Vegetatio 56:75–85

Reolid J, Bialik OM, Lindhorst S, Eisermann JO, Petrovic A, Hincke C, Beaman RJ, Webster JM, Betzler C (2024) A new type of *Halimeda* bioherm on the Queensland Plateau, NE Australia. Coral Reefs, pp 1–21

Riegl BM, Glynn PW, Wieters E, Purkis SJ, d'Angelo C, Wiedenmann J (2015) Water column productivity and temperature predict coral reef regeneration across the Indo-Pacific. Sci Rep 5(1):8273

Riegl BM, Purkis SJ, Al-Cibahy AS, Al-Harthi S, Grandcourt E, Al-Sulaiti K, Baldwin J, Abdel-Moati AM (2012) Coral bleaching and mortality thresholds in the SE Gulf: highest in the world. Coral Reefs of the Gulf: adaptation to climatic extremes, pp 95–105

Rietkerk M, van de Koppel J (2008) Regular pattern formation in real ecosystems. Trends Ecol Evol 23(3):169–175

Rietkerk M, Boerlijst MC, Van Langevelde F, HilleRisLambers R, de Koppel JV, Kumar L, Prins HH, de Roos AM (2002) Self-organization of vegetation in arid ecosystems. Am Nat 160(4):524–530

Rogers CS (1990) Responses of coral reefs and reef organisms to sedimentation. Mar Ecol Prog Ser 62(1):185–202

Rowlands G, Purkis S, Bruckner A (2014) Diversity in the geomorphology of shallow-water carbonate depositional systems in the Saudi Arabian Red Sea. Geomorphology 222:3–13

Salas-Saavedra M, Dechnik B, Webb GE, Webster JM, Zhao JX, Nothdurft LD, Clark TR, Graham T, Duce S (2018) Holocene reef growth over irregular Pleistocene karst confirms major influence of hydrodynamic factors on Holocene reef development. Quatern Sci Rev 180:157–176

Scheffer M, Carpenter S, Foley JA, Folke C, Walker B (2001) Catastrophic shifts in ecosystems. Nature 413(6856):591–596

Schlager W, Purkis SJ (2013) Bucket structure in carbonate accumulations of the Maldive, Chagos and Laccadive archipelagos. Int J Earth Sci 102:2225–2238

Schlager W, Purkis S (2015) Reticulate reef patterns–antecedent karst versus self-organization. Sedimentology 62(2):501–515

Schutter M, Crocker J, Paijmans A, Janse M, Osinga R, Verreth AJ, Wijffels RH (2010) The effect of different flow regimes on the growth and metabolic rates of the scleractinian coral *Galaxea fascicularis*. Coral Reefs 29:737–748

Sebens KP (1997) Adaptive responses to water flow: morphology, energetics, and distribution of reef corals. In: Proceedings of the 8th international coral Reef symposium, vol 2, pp 1053–1058

Simon B, Robin C, Rouby D, Braun J, Guillocheau F (2022) Estimating sediment transport diffusion coefficients from reconstructed rifted margin architecture: measurements in the Ogooué and Zambezi deltas. Basin Res 34(6):2064–2084

Stuart-Smith RD, Brown CJ, Ceccarelli DM, Edgar GJ (2018) Ecosystem restructuring along the Great Barrier Reef following mass coral bleaching. Nature 560(7716):92–96

Suosaari EP, Reid RP, Oehlert AM, Playford PE, Steffensen CK, Andres MS, Suosaari GV, Milano GR, Eberli GP (2019) Stromatolite provinces of Hamelin Pool: physiographic controls on stromatolites and associated lithofacies. J Sediment Res 89(3):207–226

Swaminathan SD, Meyer JL, Johnson MD, Paul VJ, Bartels E, Altieri AH (2024) Divergent responses of the coral holobiont to deoxygenation and prior environmental stress. Front Mar Sci 10:1301474

van de Koppel J, Crain CM (2006) Scale-dependent inhibition drives regular tussock spacing in a freshwater marsh. Am Nat 168(5):E136–E147

van de Koppel J, Rietkerk M, Weissing FJ (1997) Catastrophic vegetation shifts and soil degradation in terrestrial grazing systems. Trends Ecol Evol 12(9):352–356

van de Koppel J, Rietkerk M, van Langevelde F, Kumar L, Klausmeier CA, Fryxell JM, Hearne JW, van Andel J, de Ridder N, Skidmore A, Stroosnijder L (2002) Spatial heterogeneity and irreversible vegetation change in semiarid grazing systems. Am Nat 159(2):209–218

van de Koppel J, Rietkerk M, Dankers N, Herman PM (2005) Scale-dependent feedback and regular spatial patterns in young mussel beds. Am Nat 165(3):E66–E77

van de Vijsel RC, van Belzen J, Bouma TJ, van Der Wal D, Cusseddu V, Purkis SJ, Rietkerk M, van De Koppel J (2020) Estuarine biofilm patterns: modern analogues for Precambrian self-organization. Earth Surf Proc Land 45(5):1141–1154

van de Vijsel RC, Hernández-García E, Orfila A, Gomila D (2023) Optimal wave reflection as a mechanism for seagrass self-organization. Sci Rep 13(1):20278

van der Heide T, Bouma TJ, Van Nes EH, Van De Koppel J, Scheffer M, Roelofs JG, Van Katwijk MM, Smolders AJ (2010) Spatial self-organized patterning in seagrasses along a depth gradient of an intertidal ecosystem. Ecology 91(2):362–369

van der Kaaden AS, Mohn C, Gerkema T, Maier SR, de Froe E, van de Koppel J, Rietkerk M, Soetaert K, van Oevelen D (2021) Feedbacks between hydrodynamics and cold-water coral mound development. Deep Sea Res Part I 178:103641

van der Kaaden AS, Maier SR, Siteur K, De Clippele LH, van de Koppel J, Purkis SJ, Rietkerk M, Soetaert K, van Oevelen D (2023) Tiger reefs: self-organized regular patterns in deep-sea cold-water coral reefs. Ecosphere 14(10):e4654

van Maanen B, Coco G, Bryan KR (2015) On the ecogeomorphological feedbacks that control tidal channel network evolution in a sandy mangrove setting. In: Proceedings of the Royal Society A: mathematical, physical and engineering sciences 471(2180): 20150115

Waltham D (2008) Slope control on submarine channel widths. J Sediment Res 78(5):317–322

Williams GJ, Graham NA (2019) Rethinking coral reef functional futures. Funct Ecol 33(6):942–947

Woodhead AJ, Hicks CC, Norström AV, Williams GJ, Graham NA (2019) Coral reef ecosystem services in the Anthropocene. Funct Ecol 33(6):1023–1034

Woodroffe CD (2011) Reticulated Reefs. In: Hopley D (ed) Encyclopedia of modern coral reefs: Structure, form and process. Springer, Dordrecht

Woodroffe CD, McLean RF, Wallensky E (1994) Geomorphology of the Cocos (Keeling) Islands. Atoll Res Bull 402:1–33

Wyrwoll KH, Zhu ZR, Collins LB, Hatcher BG (2006) Origin of blue hole structures in coral reefs: Houtman Abrolhos, Western Australia. J Coastal Res 22(1):202–208

Xi H, Burgess PM, Kozlowski E, Hunt DW, Jurkiw A, Masiero I (2022) Spatial self-organization of marine agglutinated microbial carbonate build-ups: insights from stratigraphic forward modelling using Stromatobyte3D. Sed Geol 429:106081

Yamano H, Abe O, Matsumoto E, Kayanne H, Yonekura N, Blanchon P (2003) Influence of wave energy on Holocene coral reef development: an example from Ishigaki Island, Ryukyu Islands. Jpn Sediment Geol 159(1–2):27–41

Zlatarski VN, Greenstein BJ (2020) The reticulate coral reef system in Golfo de Guacanayabo. SE Cuba Coral Reefs 39(3):509–513